Continental Shelf Research 29 (2009) 1525–1534

Contents lists available at ScienceDirect

Continental Shelf Research

journal homepage: www.elsevier.com/locate/csr

Disentangling the upwelling mechanisms of the South Brazil Bight

Elbio D. Palma [a,b,*], Ricardo P. Matano [c]

[a] Departamento de Física, Universidad Nacional del Sur, Bahía Blanca, Argentina
[b] Instituto Argentino de Oceanografía, CONICET, Bahía Blanca, Argentina
[c] College of Oceanic & Atmospheric Sciences, Oregon State University, Corvallis, OR, USA

ARTICLE INFO

Article history:
Received 6 November 2008
Received in revised form
21 March 2009
Accepted 4 April 2009
Available online 16 April 2009

Keywords:
Shelf-break upwelling
Numerical modeling
South Brazil Bight

ABSTRACT

This article presents a suite of long-term numerical simulations that investigate the dynamical mechanisms controlling the circulation in the South Brazil Bight (SBB). The overarching goal of these simulations is to quantify the relative contributions of local wind forcing and the Brazil Current (BC) to the upwelling of nutrient-rich slope water onto the shelf. The model results indicate that the water mass structure of the SBB is controlled by the synergy between wind-driven, inner-shelf upwelling and geostrophic, shelf-break upwelling. The later extends yearlong but the former peaks during the austral summer and decreases towards the winter. The interaction between the poleward flow of the BC and the bottom topography greatly influences the shelf circulation, particularly in the bottom boundary layer. Changes of the SBB coastline direction and shelf width modulate the along-shore pressure gradient and the magnitude of the shelf-break upwelling and downwelling. Thus, although the summer upwelling winds extend over large part of the SBB surface temperatures are warmer in the south because of the cooling effect of the shelf-break upwelling in the northern region. At difference with previous studies of shelf-break dynamics the shelf-break upwelling in our model is not controlled by the uplifting associated with the presence of instabilities of the boundary current or nonlinear accelerations under a variable shelf width. The proposed mechanism is relatively simple. As the boundary current flows along the continental slope, changes in the coastline orientation and along-shore bottom topography modify the along-shore pressure gradient which through geostrophy leads to inshore bottom flow and hence shelf-break upwelling. Such a mechanism can provide insight into upwellings on other western boundary current regions where similar topographic variations exist.

1. Introduction

The South Brazil Bight (SBB) is a crescent-shaped shelf with a maximum width of ~200 km that is located between Cape Frio (23°S) and Cape de Santa Marta (28°40′S) (Castro and Miranda, 1998, Fig. 1). This region hosts large fisheries grounds and some of the largest oil deposits of Brazil (Matsuura, 1996; Castro et al., 2008). Its water mass structure is dominated by warm and salty Tropical Water (TW) ($T>20$ °C, $S>36.40$) in the surface and cold and relatively fresh South Atlantic Central Water (SACW) below 200 m ($T<20$ °C and $S<36.40$) (Castro and de Miranda, 1998). The surface waters are typically devoid of nutrients, but observations indicate the existence of subsurface chlorophyll values higher than 1.5 mg m^{-3} at 30–40 m. These peaks are associated with nutrient enrichment through bottom intrusions (shelf-break upwelling) of SACW carried by the Brazil Current (BC) (Brandini, 1990; Castro et al., 2008). Under persistent upwelling favorable winds the SACW can outcrop into the warmer surface coastal water creating low sea surface temperature's anomalies associated with coastal upwelling (Castelao and Barth, 2006) (Fig. 1b). These occurrences, however, are often interrupted by the passing of synoptic scale atmospheric disturbances (Castro and de Miranda, 1998).

The shelf-break upwelling of the SBB has been the focus of several observational and modeling studies, which postulated that the shelf-break upwelling is sporadic and it is related to instabilities of the mean flow (Campos et al., 1995, 2000; Castelao et al., 2004). However, recent numerical experiments indicate that this phenomenon is a persistent feature of the regional circulation (Palma et al, 2008). In this article we use the results of numerical simulations to investigate the dynamical mechanisms controlling the circulation in the SBB. Our goal is to quantify the relative contribution of local wind forcing and the BC to the upwelling of nutrient-rich slope water onto the shelf. To that end we present the results of a suite of long-term numerical simulations initialized with annual mean climatological conditions and forced with QuikSCAT winds, tides, freshwater discharges, and lateral fluxes from the results of a global, eddy-permitting numerical simulation.

* Corresponding author.
E-mail address: uspalma@criba.edu.ar (E.D. Palma).

0278-4343/$ - see front matter © 2009 Elsevier Ltd. All rights reserved.
doi:10.1016/j.csr.2009.04.002

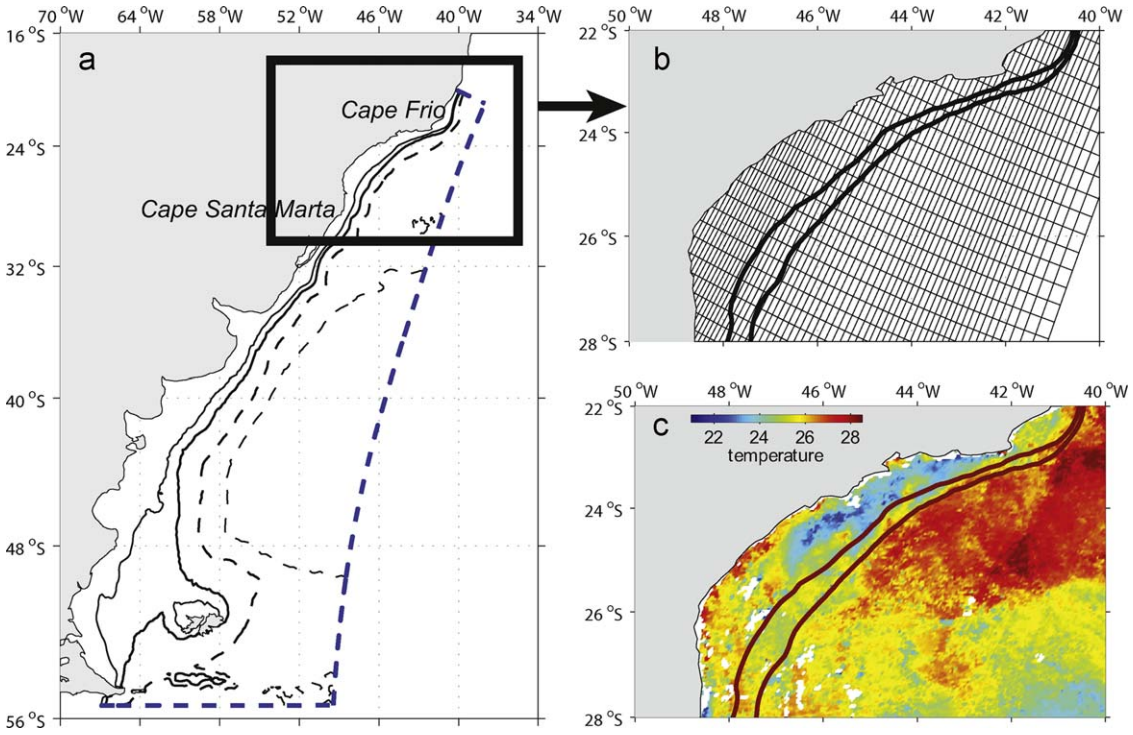

Fig. 1. (a) Location map of the South Brazil Bight (SBB) region (enclosed rectangle). The 100, 200 1000, and 4000 m isobaths are shown. The blue dashed line indicates the offshore limits of the numerical model domain. (b) Zoom of the model grid in the SBB (every 2 grid lines are shown). The heavy black lines indicate the 100 and 200 m isobaths (c) Satellite (Modis) SST in the SBB during January 2008. Note the strip of colder water ($T<23$ °C) in the northern half of the bight.

The details of the model configuration and forcing are described in Section 2. In Section 3 a description of the seasonal shelf circulation under full forcing is presented. In Section 4 the flow dynamics related to the shelf-break upwelling are examined in detail using results of experiments under different forcing and momentum analysis, and a new mechanism for upwelling is proposed. Such a mechanism can provide insight into upwellings on other western boundary current regions where similar along-shelf topographic variations exist. A summary of key findings is presented in Section 6.

2. Model description

The numerical model used in this study is the Princeton Ocean Model (Blumberg and Mellor, 1987). The model domain extends from 55°S to 18°S and from 70°W to 40°W and it has a horizontal resolution of 5 km near the western coast and 20 km near the eastern open ocean boundary (Fig. 1a). The grid orientation in most of the SBB is NE (y direction, alongshore, ~30° from true north) and SE (x direction, cross-shore) (Fig. 1b). The model bathymetry was interpolated from Smith and Sandwell (1997). The vertical resolution of the model comprises 25 vertical sigma levels with higher resolution in the top and bottom boundary layers. The model has three open boundaries were a combination of radiation and advection boundary conditions is used. The model was forced with data extracted from global models and observational databases. Tidal amplitudes and phases were interpolated from the Egbert et al. (1994) model, and boundary inflows from the POCM-4 eddy-permitting global ocean model (Tokmakian and Challenor, 1999). Heat and freshwater fluxes were parameterized with a Newtonian restoring to observed sea surface temperature (SST) and sea surface salinity (SSS) values. The former were obtained from Casey and Cornillon (1999) while the later were constructed from historical hydrographic data collected by the Argentinean Hydrographic Service. The model also includes the freshwater discharges from the La Plata River (23,000 m^3/s) and the Patos Lagoon (2000 m^3/s) (Piola et al., 2008). At the surface the model was forced with QuikSCAT wind stress scatterometer data (Risien and Chelton, 2008). Fig. 2a shows the wind stress over the SBB area during January (austral summer) and July (austral winter). The prevailing winds blow from the northeast in offshore areas and turn from the east south-east while approaching the shelf. Wind intensity shows little seasonal variations north of 27°S. However, there are seasonal changes in the wind direction in the shelf area. Fig. 2b shows the time evolution of the coastal along-shore component of the wind stress. Following Piola et al. (2008), the along-shore direction is defined as 0° from true north (28°S–25.8°S) and 45° from true north (25.8°S–23°S). During the austral summer (January–February–March) the prevailing wind direction is from the east and in the northern part of the bight (26.5°S–23°S) the winds have an important upwelling favorable component near the coast. During the austral winter (June–July–August) the winds in most of the bight blow inshore and more perpendicularly to the coastline, with null or downwelling favorable component. Recent analysis of summer QuikSCAT winds have also suggested that wind stress curl is a major contributor to the observed coldest surface water near Cape Frio (Castelao and Barth, 2006).

To characterize the annual mean circulation and seasonal variability of the SBB we use a three-year run that was initialized with annual mean temperature and salinity extracted from a World Atlas (Levitus and Boyer, 1994) and it was spun up with annual mean forcing. After reaching dynamical equilibrium this experiment was run for another six years with monthly mean forcing (EXP1). Our analysis focuses on the last three years of this simulation. For the purposes of dynamical analysis we also did an additional experiment that was initialized as EXP1 but that did not include tidal, wind, and freshwater forcing (EXP2). Thus, the deep ocean circulation is the only forcing for the shelf circulation

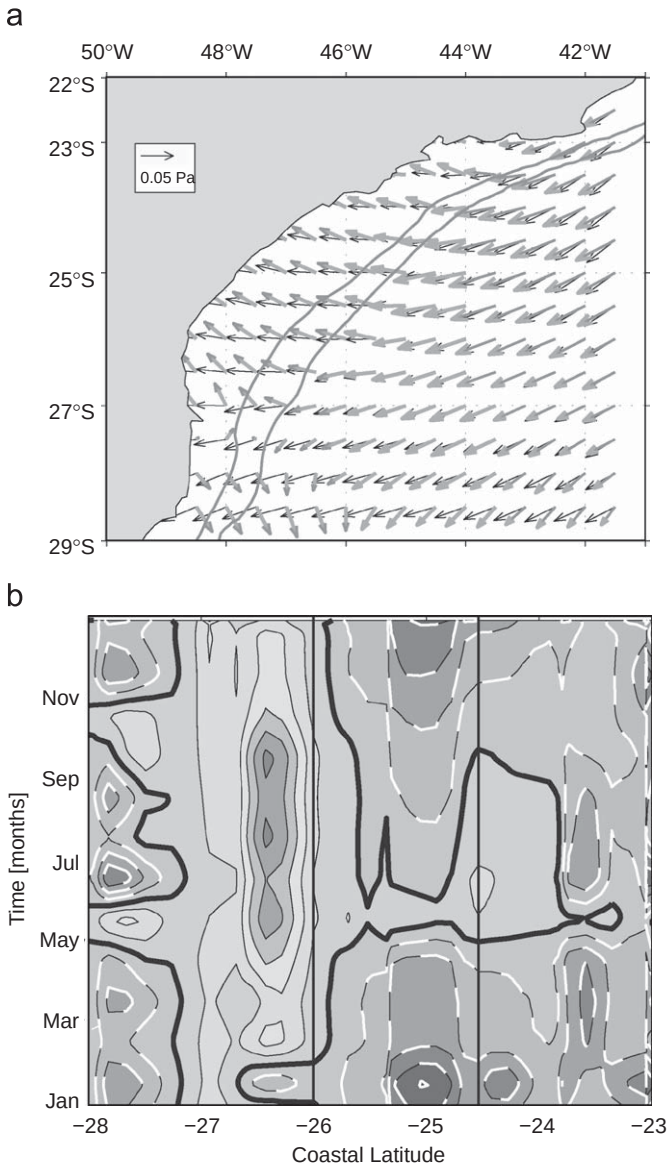

Fig. 2. QuikSCAT wind stress for summer (black arrows) and winter (heavy gray arrows) (a). Space-time plot of the coastal along-shore component of the wind stress (b). Positive values indicate downwelling favorable winds, negative values (dashed contours) indicate upwelling favorable winds.

of this experiment. Further details about the model configuration can be found in Palma et al. (2008).

3. The seasonal variability of the SBB circulation (EXP1)

The outer-shelf circulation of the SBB is highly influenced by the southward flow of the BC, which has average surface velocities at near the shelf break of 50 cm/s (Fig. 3a and b). After being forced by the abrupt change in coastline orientation near Cape Frio, the BC makes an abrupt cyclonic loop and penetrates onto the shelf whereupon it turns back to the shelf break as a southwestward flowing jet (Fig. 3a and b). The largest seasonal variations in the SBB circulation are observed in the middle and inner portions of the shelf. Currents are stronger in summer than in winter, which is consistent with the seasonal changes in the wind direction (Fig. 2). During summer they flow southwestward at an average speed of 40 cm/s (Fig. 3a). During winter the surface currents are less organized, being southwestward offshore the 90 m isobath and veering towards the coast in the inner shelf (Fig. 3b). The lack of long-term surface current measurements in the SBB precludes a proper (i.e. statistical) comparison with the results of our simulation. However, short-term current measurements in the SBB and near the shelf break showed surface velocities of the BC in agreement with the model results. Castro and Miranda (1998) reported speeds around 40–50 cm/s at 24°S; and Muller et al. (1998) showed mean surface speeds of 44.7 cm/s near 28°S.

The seasonal changes are most marked in the SST patterns. Summer SSTs are generally higher than 23 °C, except in the northwest where there is a relatively narrow ribbon of colder waters ($T\sim19$ °C) to the north of ~25°30′S (Fig. 3a). These cold waters generate a strong cross-shelf thermal front at approximately 50 km from the coast. Winter SSTs are more homogeneous, with values between 20 and 23 °C (Fig. 3b). The largest temperature gradients are observed near the shelf break and the southern portion of the bight, where the penetration of relatively cold waters ($T<19$ °C) from the south is apparent. The summer bottom temperatures show a nearly uniform distribution ($T\sim14$ °C) except in the coastal region between 26°S and 26.5°S, where temperatures are higher (Fig. 3c). Bottom temperatures are modulated by shelf-break upwelling and the advection of colder waters from Cape Frio. Piola et al. (2000) noted that between 24° and 27°S near bottom temperatures in the mid-shelf region are 2 °C consistently lower in summer than in winter (see also Matsuura, 1996). During winter, the retraction of the BC waters leads to the formation of two thermal fronts, one in the inner shelf and the other in the outer shelf that follow the bottom topography (Fig. 3d). The inner-shelf front (marked by the 17 °C isotherm) is located approximately 50 km from the coast and encloses a region with weaker bottom velocities and higher bottom temperatures. The outer-shelf front is close to the shelf break. The region between these fronts is characterized by large onshore velocities (Fig. 3d).

To complement the above description, Fig. 4 shows cross-sections of cross-shore velocities, temperature, and salinity near Santos (24°S). The cross-shelf circulation during the winter is characterized by intrusions of the BC onto the shelf (Fig. 4b). These intrusions are marked by tongues of cold and low-salinity waters in the bottom boundary layer and salty waters intruding at mid-depths (Fig. 4d and f). The temperature cross-section shows a nearly homogeneous mixed layer in the surface and a bottom thermal front located at approximately 60 km from the coast (Fig. 4d). The location where the thermocline intercepts the bottom in our numerical simulation is close to those reported by Castro et al. (2008). The salinity cross-section shows strong gradients in both the vertical and the horizontal directions. The inner-shelf is relatively fresh ($S<34.8$) and vertically homogeneous, the middle shelf shows a three-layer structure with maximum salinities at mid depth ($S>35.6$), and the outer shelf is characterized by the strong salinity front associated with the presence of the BC (Fig. 4f). Overall, the cross-shelf structure of temperature and salinity of EXP1 is in good agreement with the observations of Campos et al. (1995, 2000).

The larger penetration of the colder and less saline SACW slope waters towards the coast during the summer months is marked by the surface outcropping of the 17 °C isotherm (Fig. 4c). This indicates that the formation of the inner-shelf front described above (e.g., Fig. 3a) is related to onshore intrusions of the BC. As we shall show these cold intrusions are brought to the surface by the upwelling favorable winds that develop during this season (Fig. 2). In a nutrient poor environment the uplifting of deeper and nutrient-rich waters to the euphotic zone near the coast might be of particular importance to the local ecosystem (Castro et al., 2008). It is interesting to note that although during the summer

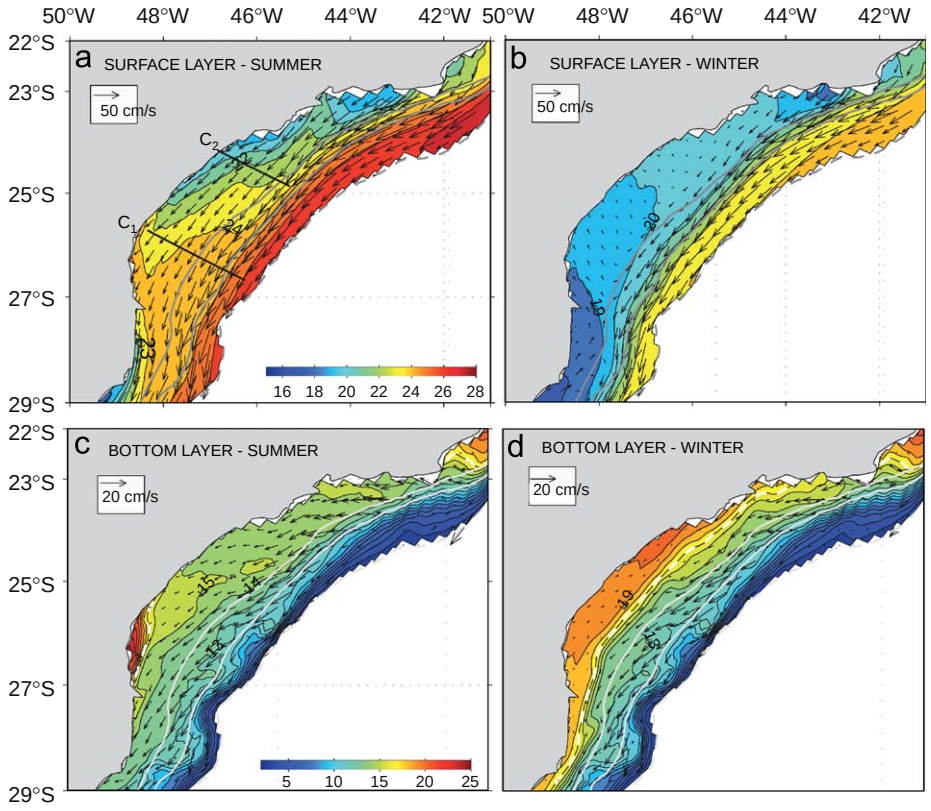

Fig. 3. Sea surface temperature and surface velocity vectors (top panels) from EXP1 and for (a) the summer and (b) the winter season. Bottom temperature and velocity vectors (bottom panels for (c) summer and (d) winter. Solid gray lines indicate the 100 and 200 m isobaths; the dashed line is the 1000 m isobath. The vector fields are shown for depths less than 1000 m. Cross sections C1 and C2 are illustrated in Figs. 4, 7, 8, 10 and 11. The white dashed-line (bottom panels) indicates the position of the 17 C isotherm.

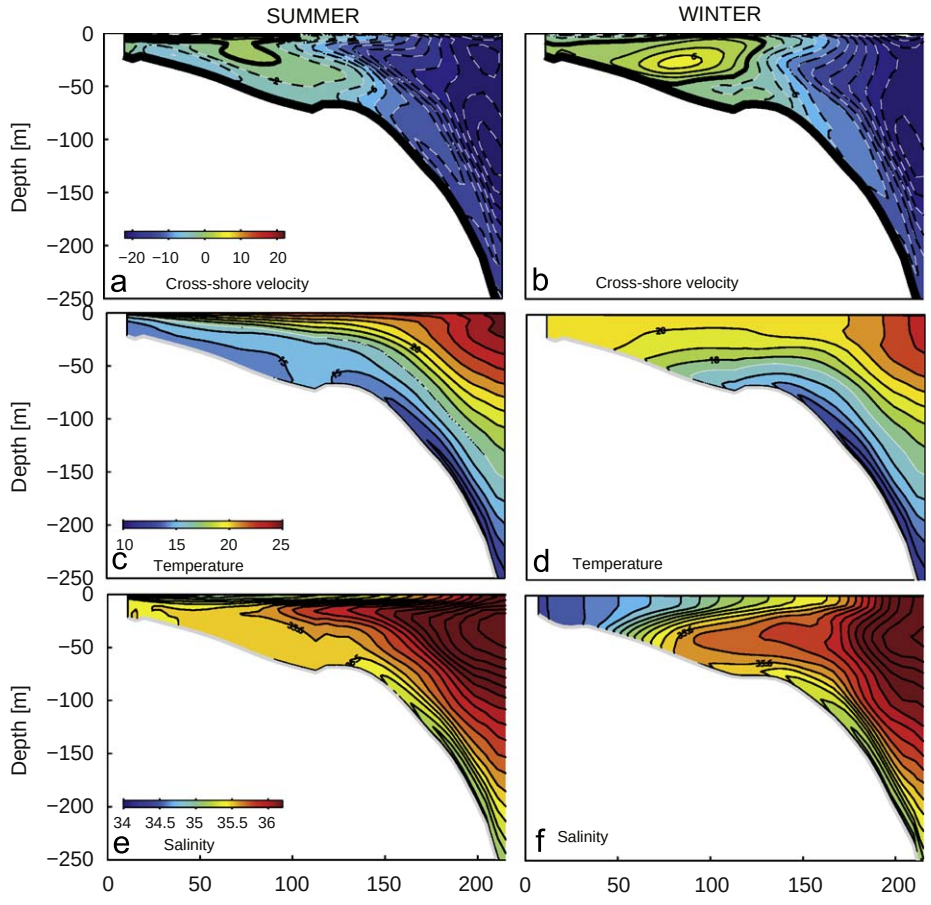

Fig. 4. Cross sections of cross-shore velocities (top panels), temperature (middle panels) and salinity (bottom panels) for cross-section C2 and for EXP1. Left panels (a), (c), (e) are results for the summer season, right panels (b), (d), (f) are for the winter season. Contour interval is 2 cm/s for panels (a) and (b), 1 °C for panels (c) and (d) and 0.1 psu for panels (e) and (f).

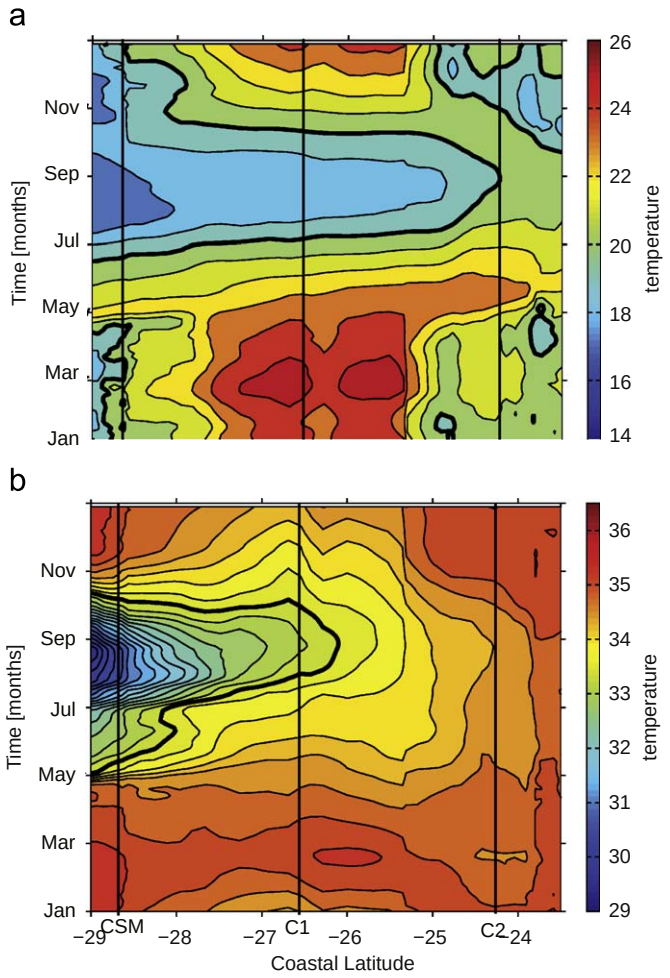

Fig. 5. (a) Space-time plot of coastal of coastal temperature (a) and salinity (b) at the SBB and from the last year of model run (EXP1). The thick black line indicates the 20 °C isotherm in (a) and the 33.5 isohaline in (b).

there is an increase of penetration of SACW in the bottom boundary layer, there is a decrease of the penetration of the salinity maximum associated with tropical waters at mid depth (Fig. 4e). It is also worth noting that the depth (~30/40 m) and offshore position (~100 km) of the cross-shelf flow convergence during the winter (Fig. 4b) that is predicted by the model is in good correspondence with the location of the deep chlorophyll maximum reported in Brandini (1990) and Castro et al. (2008).

The dominance of the seasonal cycle on the variability of the coastal circulation and water mass structure is illustrated by Hovmöller diagrams of nearshore SSTs and SSSs (Fig. 5). The summer (January–March) SSTs show two well-defined regions: the southern region of the bight (27.5°S–25.5°S), which has maximum temperatures of 25 °C, and the northern region where temperatures drop below 21 °C (Fig. 5a). The crowding of the isotherms near 25.5°S indicates the place of the largest temperature changes with a range of approximately 5 °C, while south of 27.5°S the temperature shows a smoother transition. The marked decrease of summer SSTs in the northern half of the bight is related to the onset of upwelling favorable winds during this season (Fig. 2b). However, while the band of upwelling favorable winds extends south of 25.5°S (Fig. 2b) the SST distribution shows relatively warm waters as far as 28°S, suggesting that the wind seasonal changes alone cannot account for the modeled SST structure. As we shall show coastal SSTs are not only modulated by the local winds but also by the onshore intrusions of the BC. The homogeneous distribution of winter SSTs is only disturbed by cold, southerly intrusions during August ($T<19$°C). The winter intrusion of cold water tongues are also observed in historical hydrographic data (Castro and de Miranda, 1998) and satellite SST images (Campos et al., 2000). The SSS distribution shows the largest variations during the winter (Fig. 5b), with the appearance of a low-salinity tongue ($S<33.5$) that is associated with the freshwater discharges from the La Plata River. The northernmost limit of the freshwater plume (marked by the 33.5 psu isohaline), reaches its maximum extent at ~26°S in mid-winter. The expansion and retraction velocity of the freshwater discharge in our simulation are in good agreement with satellite chlorophyll_a data (CSAT, Piola et al., 2008).

4. Dynamical analysis

The water mass structure of the SBB is modulated by onshore intrusions of the BC and coastal wind-driven upwelling. To quantify the relative contribution of each of these types of upwelling to the SBB water mass structure we did an ancillary experiment (EXP2) using the same model set-up than EXP1 but without tidal, freshwater, and wind stress forcing. Thus, in EXP2 the departures of the temperature and salinity fields from their initial conditions are largely attributed to the influence of the BC on the shelf region.

To characterize the differences between EXP1 and EXP2 Figs. 6 and 7 display horizontal and cross-shelf sections of the initial state and the two experiments. In the initial state SSTs are nearly uniform throughout the domain while the bottom temperatures decrease towards the shelf break (Fig. 6a and b). The 17 °C isotherm, which marks the division between the cold SACW waters carried by the BC and the warmer shelf waters roughly follows the 200 m isobath (Figs. 6b and 7a). The middle panels of Figs. 6 and 7 show the results of EXP2. The surface circulation is dominated by the strong southwestward flow of the BC over the continental slope and a weak flow inshore of the 100 m isobath (Fig. 6c). The SST field is nearly uniform over the shelf with a slight increase of temperatures towards the shelf break (Fig. 6c). The differences with the initial conditions are associated with the summer heating of the surface layer and the southward advection of warmer tropical waters by the BC. The bottom temperatures show an overall drop of ~5 °C from their initial state (Fig. 6d), with a marked along-shelf gradient that is characterized by higher values in the south. The contribution of the BC intrusions to the shelf water mass structure is better appreciated in the cross-shelf sections (Fig. 7c and d). Note, for example, the uplift of the 17 °C isotherm, which marks the limit between the shelf waters and the SACW in the initial fields from its initial position near the 200 m isobath to a depth of 40 m throughout the shelf (Fig. 7c). A similar effect is observed in the salinity field (Fig. 7d).

The influence of the wind stress forcing on water mass structure of the SBB can be elucidated from the comparison of EXP1 and EXP2 (Fig. 7e and f). Upwelling favorable winds in EXP1 further entrain the relatively cold waters of the BC onto the inner shelf and force the outcrop of deep, cold waters in the coastal region (Fig. 7e). This effect is also appreciated in the salinity field, which shows a coastal progression of more saline water and the offshore displacement of surface low-salinity waters (Fig. 7f). The wind-driven upwelling sustains the inner-shore SST front described in the previous section (e.g., Fig. 3a).

To quantify the influence of local (winds) and distant (BC) forcing to the cross-shelf variability of the temperature and salinity fields we computed profiles of the depth averaged temperature (Tm) and bottom salinity of EXP1 and EXP2 during the winter and summer seasons. With the exception of EXP1 in

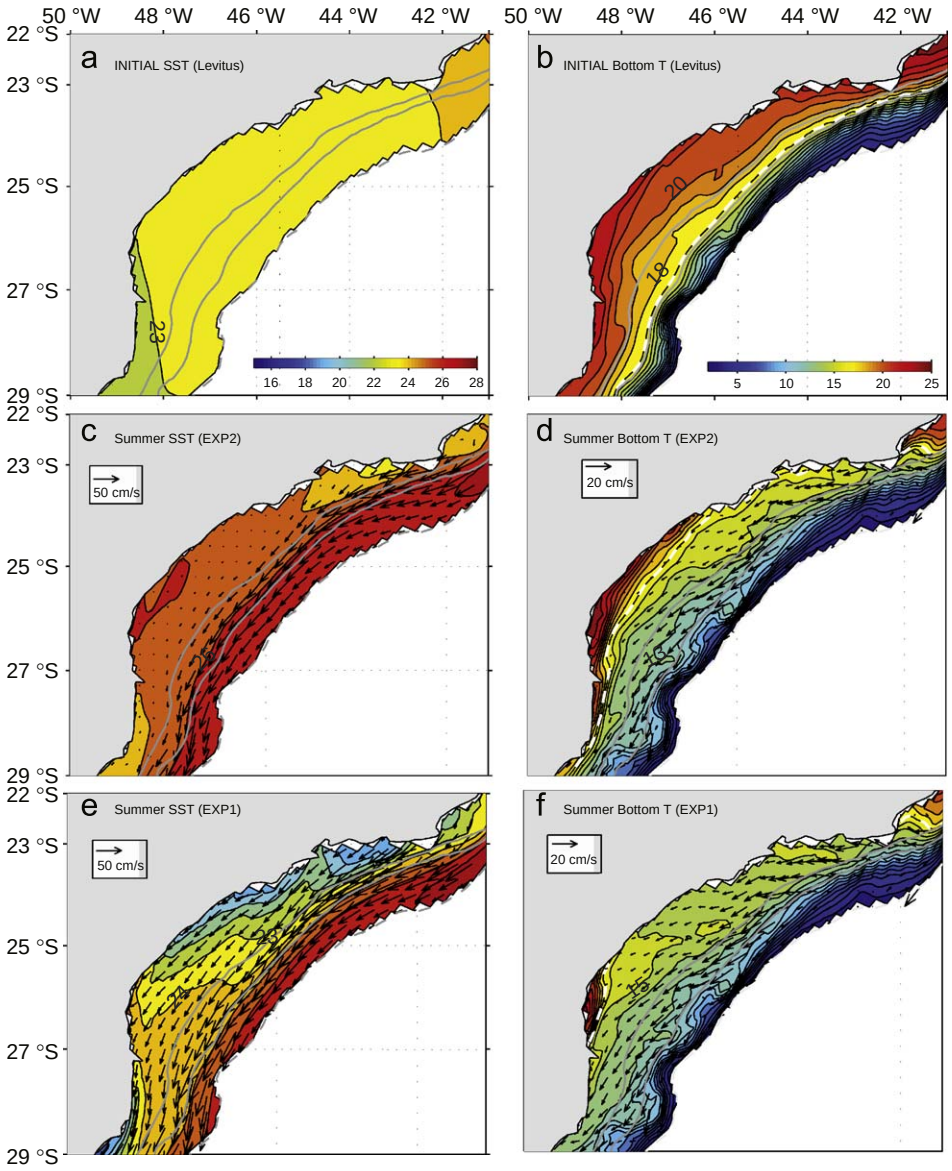

Fig. 6. Sea surface temperature and surface velocity vectors for the summer season (left panels): (a) Initial condition, (c) EXP2 results, (e) EXP1 results. Bottom temperature and velocity vectors (right panels) :(b) initial condition, (d) EXP2 results, (f) EXP1 results. The gray lines indicate the 100 and 200 m isobaths. The white dashed line (right panels) indicates the position of the 17 °C isotherm.

summer, the largest departures from the initial temperature profile (∼−4°C) for both experiments is observed near the shelf break (Fig. 8a). The further drop of Tm near the coast in EXP1 is driven by the effect of the summer northeasterly winds, which upwell colder bottom water and lower the inner-shelf Tm. During the winter, vertical mixing generated by downwelling winds increase Tm to a value that is slightly higher than that of EXP2 (note the homogenized cross-shelf temperature in Fig. 4d). The seasonal variations of Tm in the inner shelf in EXP2 are largely due to changes in the atmospheric heat flux since the model BC at this latitude shows weak seasonal variations of its transport. The bottom salinity shows an overall freshening tendency, except during the winter months in EXP1 (Fig. 8b). Then, the downwelling winds isolate the outer shelf from the inner shelf creating a sharp salinity gradient at approximately 70 km from the coast.

To identify the dynamical mechanisms that control the model circulation in the SBB we calculated the momentum balances in the bottom boundary layer for EXP1 and EXP2 (Appendix A). Our discussion will be centered in the along-shelf component of this balance because the cross-shelf component is largely dominated by the geostrophic equilibrium. The momentum balance of EXP2 is dominated by vertical diffusion, the along-shelf pressure gradient and the Coriolis term (Fig. 9). Their spatial variations identify the dynamical mechanisms that regulate the shelf-break upwelling in the different portions of the domain. In the north the balance is controlled by the along-shelf pressure gradient, which, through geostrophic equilibrium, generates strong inshore velocities and hence shelf-break upwelling (Figs. 9 and 10a, gray lines). As noted in Palma et al. (2008) this particular balance reflects the along-shelf variations of the coastline and bottom topography since without them a classical Ekman balance between vertical diffusion and the Coriolis term would dominate the bottom boundary layer. Coastline orientation changes in the southern portion of the SBB lead to a change of sign of the along-shore pressure gradient and hence to offshore velocities (i.e. downwelling) in the bottom boundary layer. However, this effect is not ubiquitous because the narrowing of the shelf also leads to an increase of the vertical mixing which sometimes (i.e. under

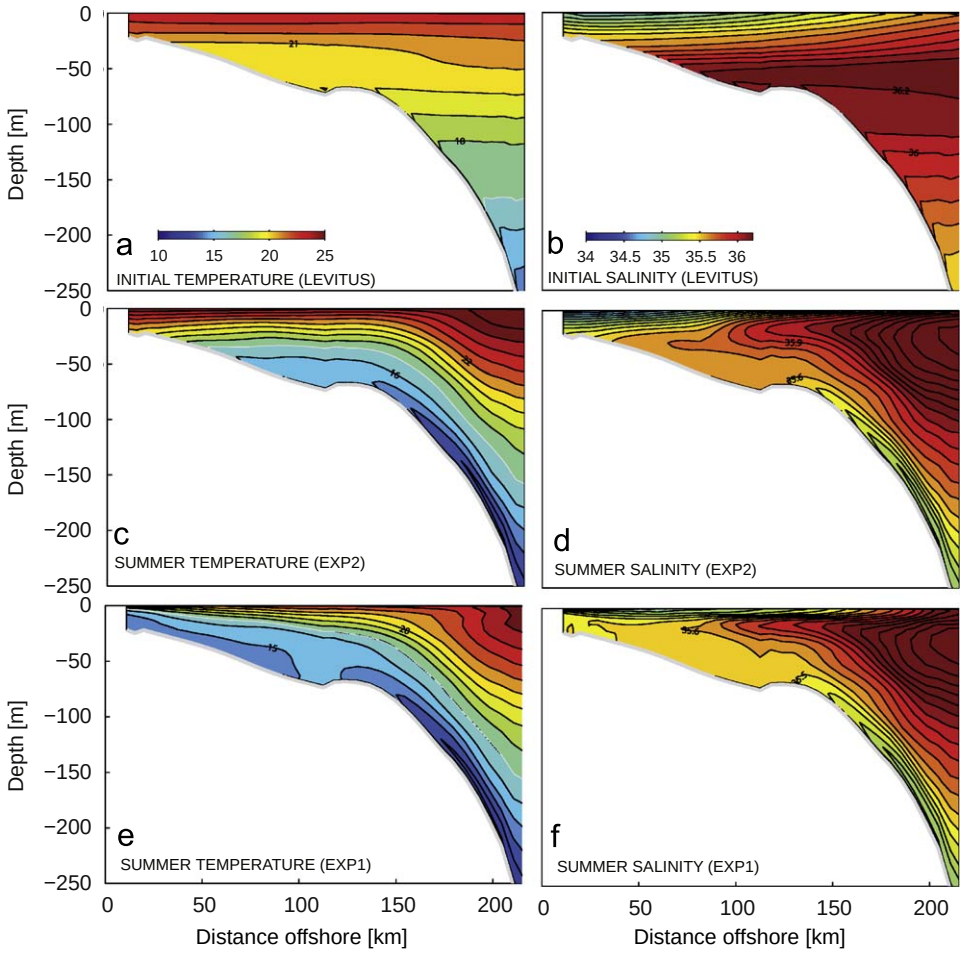

Fig. 7. Cross-sections of temperature (left panels), and salinity (right panels) for cross-section C2 Top panels (a) and (b) are the model initial condition, (c) and (d) are results from EXP2, (e) and (f) are from EXP1.

upwelling winds) might overcome the pressure gradient effect and generates weak shoreward flow (Fig. 11).

The contribution of the wind stress forcing to the momentum balance are illustrated in cross-sections of EXP1 corresponding to the northern and southern portions of the SBB (Figs. 10 and 11). During the summer, the wind stress forcing in the northern portion of the basin increases the onshore velocities in the inner shelf (Fig. 10a, black lines). Slope water is funneled from the deep ocean onto the shelf and upwelled in the near coastal region (Fig. 7e). The minor seasonal changes observed in the middle- and outer-shelf upslope flow in EXP2 (gray lines) are driven by the model weak seasonal changes in the magnitude of the BC which in turn impact on the along-shore pressure gradient at the shelf break. In the southern region, although the pressure gradient changes sign, the addition of wind forcing leads to an increase in vertical mixing and there is also inshore flow at the shelf break (Fig. 11). The downwelling favorable winds during the winter produce an offshore flow in the BBL of the inner shelf (Fig. 10b). The zero crossing of the *fu* curve in Fig. 10b, marks the location of the bottom thermal and salinity front (Fig. 4, right panels), which is a region of convergence of the bottom velocities and hence upwelling.

5. Summary and conclusions

Our numerical experiments indicate that the water mass structure of the SBB is controlled by the synergy between the inner-shelf, wind-driven upwelling and the shelf-break geostrophic upwelling. The former peaks during the austral summer and decreases towards the winter while the later extends yearlong. The circulation patterns and density structures derived from the numerical simulations correspond well with observations (Castro and de Miranda, 1998; Campos et al., 2000) and previous numerical simulations (Castelao et al., 2004). It should be noted that although our model has substantial eddy variability, it lacks the resolution needed to properly represent cross-shelf eddy fluxes and therefore we have not quantified the relative importance of eddy-driven upwelling.

The interaction between the poleward flow of the BC and the bottom topography greatly influences the nearshore circulation, particularly in the bottom boundary layer. Changes of the SBB width modulate the alonghsore pressure gradient and the magnitude of the shelf-break upwelling and downwelling. Thus, although the summer upwelling winds extend over most the SBB the SSTs are warmer in the south because of the cooling effect of the shelf-break upwelling in the northern region (Figs. 5a and 9c). As noted in the previous section the narrowing of the shelf in the southern portion of the bight leads to an enhancement of the vertical mixing that in some situations (e.g., when there is an increase in the BC transport or the magnitude of the wind stress forcing) can overcome the unfavorable along-shore pressure gradient and promote upwelling.

The generation of shelf-break upwelling by cyclonic boundary currents is a common phenomenon that is observed in the South

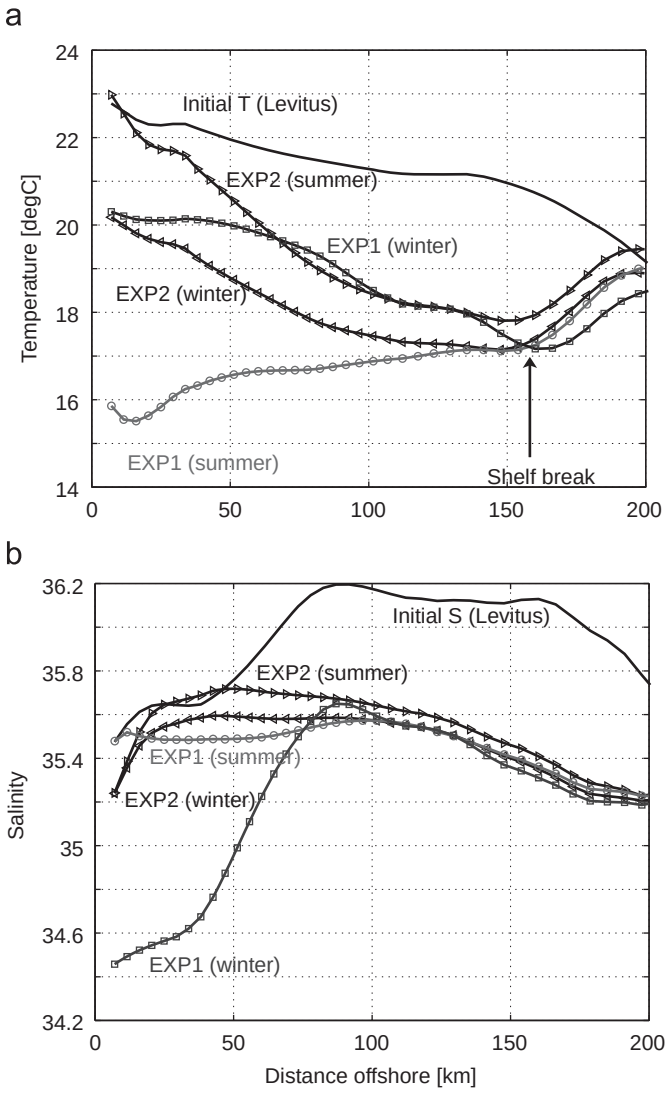

Fig. 8. Depth-mean temperature (a) and bottom salinity (b) at cross section C2.

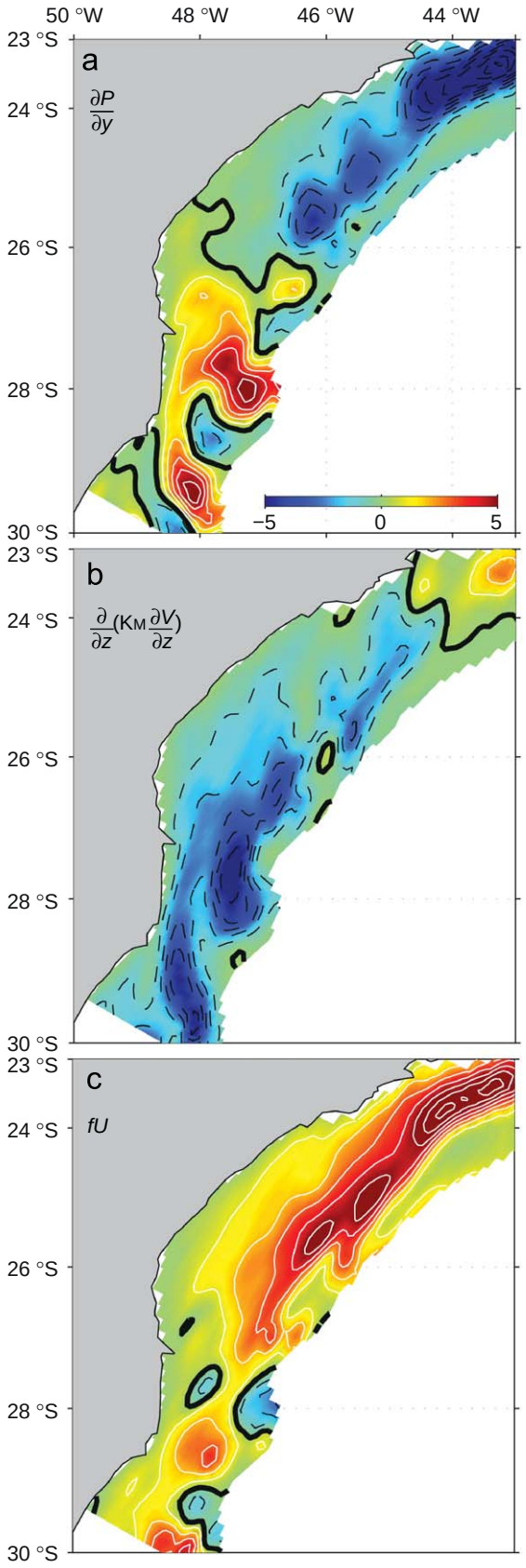

Fig. 9. The along-shelf momentum balance in the South Brazil Bight BBL and for EXP2. (a) along-shelf pressure gradient (b) vertical mixing (c) Coriolis term. Note that positive *fu* indicates onshore flow.

Atlantic Bight (SAB, Boicourt et al., 1998), the southeastern coast of Africa (Lutjeharms et al., 1989), and off eastern Australia (Roughan and Middleton, 2002). Numerical simulations presented by Oke and Middleton (2000, 2001) revealed that the narrowing of the eastern Australian shelf cross-section advectively accelerates the East Australian Current (EAC) increasing the bottom stress on the shelf and slope, which in turn acts to drive onshore flow through the bottom boundary layer. In spite of the geographical differences with the SBB the upwelling mechanism proposed by Oke and Middleton (2000, 2001) is dynamically consistent with that postulated herein, the key element in both analysis being the along-shore variation of the bottom topography. An increase in bottom stress in regions where the BC finds a narrower shelf can be seen in Fig. 9b near Cape Santa Marta. However, it is only in the northern half of the SBB, where the along-shelf pressure gradient is favorable (Fig. 9a), that there is substantial onshore bottom flow. In the southern sector, bottom friction, although more important than in the north, is not capable to overcome the adverse pressure gradient set-up by the change in orientation of the isobaths (Fig. 11, EXP2). The enhanced friction brought by the summer upwelling winds in this sector however, is enough to drive a weak onshore bottom flow (Fig. 11, EXP1). Note that the results presented by Oke and Middleton (2000, 2001) showed an increase in shelf-break upwelling promoted by the EAC

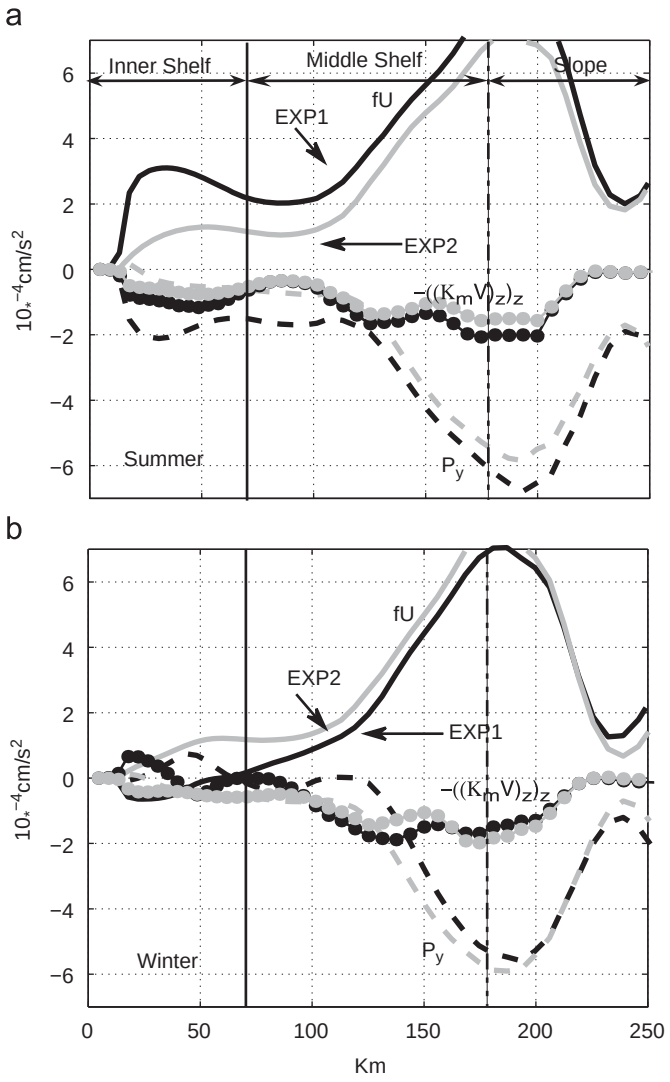

Fig. 10. Along-shelf momentum balance in the BBL for cross-section C2 (Northern SBB) in summer (a) and winter (b). Black lines are results from EXP1, gray lines are results from EXP2. fU indicates the Coriolis term, P_y indicates the along-shelf pressure gradient and $((K_MV)_z)_z$ indicates the vertical mixing term.

downstream of diverging isobaths, and some indication of the importance of the favorable along-shore pressure gradient in the bottom boundary layer in these areas is given in their momentum analysis (Oke and Middleton, 2000, their Fig. 12, right bottom panel).

Campos et al. (2000) and Castelao et al. (2004) ascribed the SBB shelf-break upwelling to the passage of meanders and eddies produced by instabilities of the BC. We argue that these perturbations are not necessary to explain the observed uplifting of the isopycnals which, according to the proposed model, is modulated by the coastal geometry. Along-shore changes in the bottom topography modify the meridional pressure gradient associated with the BC and lead to inshore bottom flow and hence shelf-break upwelling. To support our explanation we would like to note that there is no observational evidence that the meandering of the BC, postulated by Campos et al. (2000) and Castelao et al. (2004), should favor more upwelling on the northern sector of the bight, as the observations and our model results confirm. Thus, the shelf-break upwelling in the proposed model is not associated to the influence of instabilities of the boundary current or nonlinear accelerations of the current under a variable shelf width but to changes of the alonghsore pressure

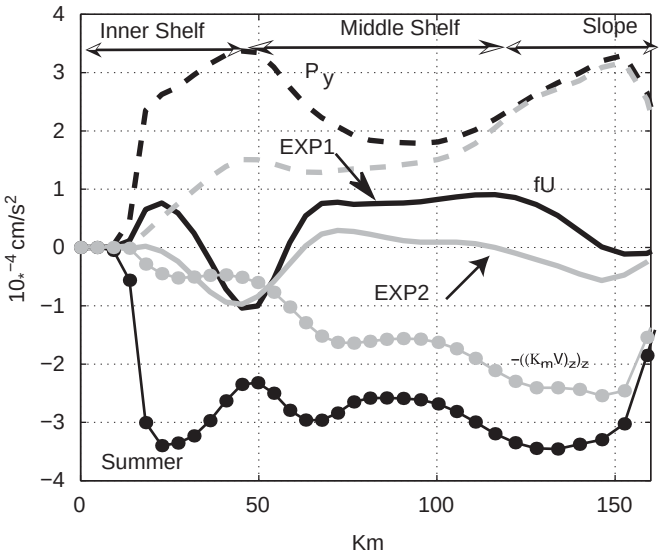

Fig. 11. Along-shelf momentum balance in the BBL for cross-section C1 (Southern SBB) in summer. Black lines are results from EXP1 and gray lines are results from EXP2.

gradient associated to changes in bottom topography. Nevertheless, it should be noted that the different models of upwelling are not mutually exclusive but, in fact, might reinforce each other. The difference, however, is that while the upwelling modes generated by eddies and meanders (like the Gulf Stream) or encroachment (like the EAC) are sporadic, the one generated by the interaction between the western boundary currents and the bottom topography through modification of the along-shore pressure gradient or enhanced bottom friction is a persistent phenomenon.

Acknowledgments

Support for E. D. Palma came from Agencia Nacional de Promoción Científica y Tecnológica (ANCYPT-Grant PICT04-25533), CONICET (Grant PIP04-6138) and by Collaborative Research Network grant CRN2076 from the Inter-American Institute for Global Change Research, supported by the US National Science Foundation grant GEO-0452325. E. D. P. acknowledges partial support by Universidad Nacional del Sur (Grant F032). R. P. Matano acknowledges the support of NSF Grant OCE-0726994, NASA Grant NNX08AR40G and JPL contract 1206714. This paper benefited substantially from comments and suggestions given by Alberto R. Piola and an anonymous reviewer. The authors would like to thank Roberto Venegas for kindly providing the satellite data used in Fig. 1c.

Appendix A

Momentum balance.

$$\underbrace{\frac{1}{D}\frac{\partial(D\vec{V})}{\partial t}}_{\text{Tendency}}+\underbrace{\vec{f}\times\vec{V}}_{\text{Coriolis}}+\underbrace{g\nabla P}_{\text{Pressure gradient}}+\underbrace{\frac{1}{D}\frac{\partial}{\partial\sigma}\left[\frac{K_M}{D}\frac{\partial\vec{V}}{\partial\sigma}\right]}_{\text{Vertical diffusion}}+\underbrace{A}_{\text{Advection and horiz. diff.}}=0$$

where $\vec{V}$is the horizontal velocity vector, $\vec{f}=f\vec{k}$ de Coriolis vector, P the pressure, D the water depth, K_M the coefficient of vertical viscosity, and A encompasses all the terms related to advection and horizontal diffusion. The pressure gradient is split into

barotropic and baroclinic pressure gradients computed as

$$\nabla\eta = \left[\frac{\partial\eta}{\partial x}, \frac{\partial\eta}{\partial y}\right]^T$$

$$\nabla\phi = \left[\frac{\partial\phi}{\partial x}, \frac{\partial\phi}{\partial y}\right]^T = \frac{D}{\rho_o}\int_\sigma^0 \left[\frac{\partial\rho}{\partial x} - \frac{\sigma}{D}\frac{\partial D}{\partial x}\frac{\partial\rho}{\partial\sigma}, \frac{\partial\rho}{\partial y} - \frac{\sigma}{D}\frac{\partial D}{\partial y}\frac{\partial\rho}{\partial\sigma}\right]^T d\sigma$$

where η is the free surface elevation and ρ the density.

References

Blumberg, A.F., Mellor, G.L., 1987. A description of a three-dimensional coastal ocean circulation model. In: Heaps, N. (Ed.), Three-Dimensional Coastal Ocean Models, Coastal and Estuarine Sci. Ser., Vol. 4. American Geophysical Union, Washington DC, pp. 1–16.

Boicourt, W.C., Wiseman Jr., W.J., Valle-Levinson, A., Atkinson, L.P., 1998. Continental shelf of the southeastern United States and the Gulf of Mexico in the shadow of the western boundary current. In: Robinson, A.R., Brink, K.H. (Eds.), The Sea, Vol. 11. Wiley, New York, pp. 135–182.

Brandini, F.P., 1990. Hydrography and characteristics of the phytoplankton in shelf and oceanic waters off southeastern Brazil during winter (July/August 1982) and summer (February/March 1984). Hydrobiologia 196, 111–148.

Campos, E.J., Goncalves, J., Ikeda, Y., 1995. Water mass characteristics and geostrophic circulation in the South Brazil Bight: summer of 1991. Journal of Geophysical Research 100, 18,537–18,550.

Campos, E.J., Velhote, D., da Silveira, I.C., 2000. Shelf break upwelling driven by Brazil Current cyclonic meanders. Geophysical Research Letters 27 (6), 751–754.

Casey, K.S., Cornillon, P., 1999. A comparison of satellite and in situ based sea surface temperature climatologies. Journal of Climate 12, 1848–1863.

Castelao, R.M., Campos, E.J.D., Miller, J.L., 2004. A modeling study of coastal upwelling driven by wind and meanders of the Brazil current. Journal of Coastal Research 20 (3), 662–671.

Castelao, R.M., Barth, J.A., 2006. Upwelling around Cabo Frio, Brazil: the importance of wind stress curl. Geophysical Research Letters 33, L03602.

Castro, B.M., Miranda, L.B., 1998. Physical oceanography of the western Atlantic continental shelf located between 4°N and 34°S. In: Robinson, A.R., Brink, K.H. (Eds.), The Sea, vol. 11. Wiley, New York, pp. 209–251.

Castro, B.M., Brandini, F.P., Pires-Vanin, A.M.S., Miranda, L.B., 2008. Multidisciplinary oceanographic processes on the western atlantic continental shelf between 4°N and 34°S. In: Robinson, A.R., Brink, K.H. (Eds.), The Global Coastal Ocean: Interdisciplinary Regional Studies and Syntheses, Pan-Regional Syntheses and the Coasts of North and South America and Asia, The Sea, Vol. 14A. Harvard University Press, Cambridge, MA Part 2, Chapter 8.

Egbert, G.D., Bennet, A.F., Foreman, M.G., 1994. TOPEX/POSEIDON tides estimated using a global inverse model. Journal of Geophysical Research 99, 24,821–24,852.

Levitus, S., Boyer, T.P., 1994. World Ocean Atlas 1994, vol. 4, Temperature, NOAA Atlas NESDIS, vol. 4. NOAA, Silver Spring, MD, 129pp.

Lutjeharms, J.R.E., Gründlingh, M.L., Carter, R.A., 1989. Topographically induced upwelling in the Natal Bight. South African Journal of Science 85, 310–316.

Matsuura, Y., 1996. A probable cause of recruitment failure of the Brazilian sardine *Sardinella aurita* population during the 1974/75 spawning season. South African Journal of Marine Science 17, 29–35.

Muller, T.J., Ikeda, Y., Zangenberg, N., Nonato, L.V., 1998. Direct measurements of western boundary currents off Brazil between 20°S and 28°S. Journal of Geophysical Research 103, 5429–5437.

Oke, P.R., Middleton, J.H., 2000. Topographically induced upwelling off Eastern Australia. Journal of Physical Oceanography 30, 512–531.

Oke, P.R., Middleton, J.H., 2001. Nutrient enrichment off Port Stephens: the role of the East Australian current. Continental Shelf Research 21, 587–606.

Palma, E.D., Matano, R.P., Piola, A.R., 2008. A numerical study of the Southwestern Atlantic Shelf circulation: stratified ocean response to local and offshore forcing. Journal of Geophysical Research 113, (C11010), doi:10.1029/2007JC004720.

Piola, A.R., Campos, E.J.D., Moller, O.O., Charo, M., Martinez, C., 2000. Subtropical shelf front off eastern South America. Journal of Geophysical Research 105 (C3), 6566–6578.

Piola, A.R., Romero, S.I., Zajaczkovski, U., 2008. Space-time variability of the Plata plume inferred from ocean color. Continental Shelf Research 28, 1556–1567.

Risien, M.R., Chelton, D.B., 2008. A global climatology of surface wind and wind stress fields from 8 years of QuikSCAT scatterometer data. Journal of Physical Oceanography 38 (11), 2379–2413.

Roughan, M., Middleton, J.H., 2002. A comparison of observed upwelling mechanisms off the east coast of Australia. Continental Shelf Research 22, 2551–2572.

Smith, R.D., Sandwell, D.T., 1997. Global sea floor topography from satellite altimetry and ship depth soundings. Science 277, 1956–1962.

Tokmakian, R., Challenor, P., 1999. On the joint estimation of model and satellite sea surface height anomaly errors. Ocean Modelling 1, 39–52.